

Small fermionic systems: the common methods and challenges

E. Suraud¹ and P.-G. Reinhard²

¹ Laboratoire Physique Théorique, Université Paul Sabatier, 118 Route de Narbonne, 31062 Toulouse cedex, France

² Institut für Theoretische Physik, Universität Erlangen, Staudstrasse 7, D91058 Erlangen, Germany

Abstract. We present a brief review of some static and dynamical properties of metal clusters, addressing various dynamical regimes, from the linear to the non linear domain. We emphasize relations with atomic nuclei and focus on cluster quantities which have counterparts in nuclei. We discuss the case of the optical response which provides a key tool of analysis of the structure and shape of simple metal clusters. We also discuss emission properties of irradiated metal clusters and show kinetic energy spectra of emitted electrons as well as angular distributions thereof.

*This contribution is summarizing results presented in two previously published papers (J. Navarro et al, Euro. Phys. J. A **30** (2006) 333 and P.-G. Reinhard et al, Int. J. Mod. Phys E **15** (2006) 1549).*

1 Introduction

The scope of this contribution is a rapid survey of some static and dynamical properties of metal clusters emphasizing observables which can be related to similar ones in nuclei. Both systems have indeed much in common. Both their structure and dynamics are dominated by the behaviour of Fermion liquids: the protons and neutrons in nuclei and the dense electron cloud in clusters. It is known since long that Fermi liquids constitute one of the basic states of matter [1]. They are furthermore highly correlated systems which, however, never freeze out to a crystalline state precisely due to the strong Fermi correlation. Nuclei and metal clusters have a well defined saturation density with low compressibility which makes that the finite drops share several key features. One can in particular cite the scaling of radius with size ($R \propto N^{1/3}$), shell effects and corresponding deformation pattern [2, 3], what concerns static properties. But there also exists similar dynamical features, such as pronounced resonance excitations related to zero sound in homogeneous matter, the giant resonances in nuclei and the surface plasmon in clusters [2–4]. Finally, one can mention, fusion/fission [5] as a further aspect in the case of large amplitude collective motion.

In both systems (nuclei and metal clusters) the strong correlations can hardly be dealt with in detail, so that effective energy-density functionals are employed for self-consistent calculations of ground state and dynamics, see e.g. [6] for the electrons in clusters, and [7] for nuclei. This short list of basic properties shows that nuclei and metal clusters have much in common. But there are also several noteworthy differences, for example concerning composition. Mind that while nuclei are composed of particles of similar masses, metal clusters contain both electrons and ions which induces the coexistence of very different time scales. It is thus most interesting to discuss these systems in comparison.

We shall confine the present analysis to some basic structural and dynamical aspects focusing on quantities which exist in both systems. Most prominent and much studied are the resonance modes. This concerns the Mie plasmon in the case of clusters. We shall show that this mode brings a bunch of relevant information, especially for our understanding of structure and shape of metal clusters. These modes can be accessed by photoabsorption measurements. They belong to small amplitude oscillations (for a general overview on small oscillations in Fermion systems see [4]). A survey treating resonance modes in nuclei, metal clusters, and liquid ^3He drops was also given in [8–11]. Dynamics will be addressed through the analysis of electronic emission after laser irradiation. We shall mostly discuss photoelectron spectroscopy which gives access to single electron level energies. Emitted electrons can be analyzed both in terms of their energy and direction of emission. We shall show examples of both observables. Before addressing these various points, as well as briefly presenting the theoretical framework, we first give a quick survey of what kind of observables can be attained in clusters.

2 Experimental signals from metal clusters

Metal clusters are usually formed in sources which produce a distribution of clusters of various masses and temperatures [12]. A direct access to well defined masses is thus not easy which makes the handling of clusters delicate. The proper tuning of the cluster source thus constitutes a key step in cluster physics. The quality of source handling thus sets limitations to what is finally accessible on a given cluster. For sake of simplicity in the forthcoming discussions we shall nevertheless consider here that this prerequisite is properly fulfilled, namely that one has at hand, for experiments, a well defined set of clusters of a given mass. We shall furthermore assume that the cluster temperature is reasonably low to avoid questions linked to solid-liquid phase transitions. Such a situation is fortunately nowadays attained in many experiments.

Lasers provide a basic tool for investigations of clusters. The laser field ionizes the cluster, which allows an easy electromagnetic handling of the thus formed cluster ion. The response of the cluster may involve several signals, depending on the degree of ionization, as sketched in figure 1. Basic signals are provided by photons, electrons and clusters themselves. Analysis in terms of photon energies (photoabsorption cross sections) provide the so called optical response, which is the cluster analogon of giant resonances in nuclei. As we shall see the optical response provides

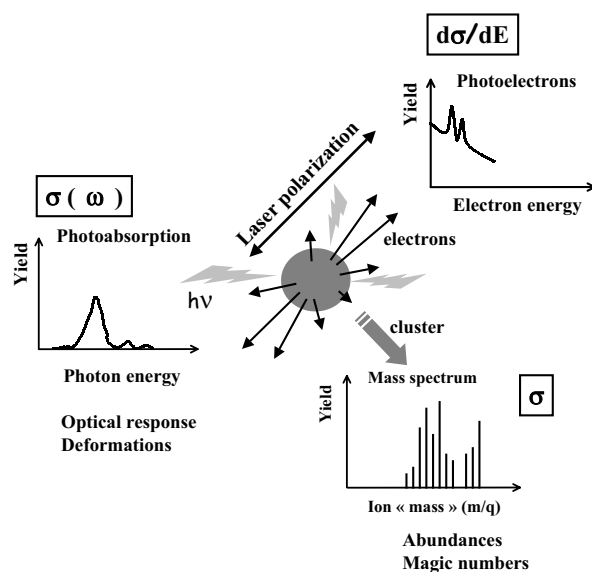


Figure 1. Schematic illustration of basic observables accessible in standard experiments on metal clusters. Measurements after a cluster irradiation may involve photons (left panel with a photoabsorption cross section $\sigma(\omega)$, as a function of laser frequency ω), electrons (upper right panel with a photoelectron spectrum, which is a differential cross section as a function of electron kinetic energy $d\sigma/dE$) or clusters themselves (right bottom panel with a mass spectrum, which is an averaged cross section σ). All these quantities provide complementing information on cluster properties. See also text for details.

a key tool of analysis of cluster structure and shapes. Electrons emitted after laser irradiation (photoelectrons) can be analyzed with various degrees of sophistication. The mere total number gives access to the net cluster charge which already provides a basic indicator on the degree of violence of the interaction process. The measurements of cluster mass spectra also bring interesting information especially in terms of abundances and are thus of great use for identifying shell closure effects, as in the nuclear case. The analysis of kinetic energies of emitted electrons provides a richer indicator useful for both structure and dynamical questions. We shall discuss it in some detail below.

3 Nuclei and metal clusters

3.1 More similar than different ?

Nuclei and the electron cloud of metal clusters are dense fermion systems exhibiting strong Pauli correlations. To make this qualitative analogy more quantitative let us briefly recall a few key characteristics of metal clusters (in relation to nuclei),

concerning, in particular, dominant interactions, sizes, structure and dynamics. In metal clusters, the Coulomb interaction plays the key role. The repulsive interaction between electrons is compensated by the attraction to (positively charged) ions. It is by the way interesting to note that in a neutral cluster, most of the binding actually results from the electronic exchange and correlation part of the interaction. In nuclei, the binding is dominated by the short range nuclear interaction which is generally larger than the Coulomb interaction. Still, the two systems furthermore exhibit a similar "saturating" behavior with radii scaling with the power 1/3 of the size of the system. The proportionality factor is known in metal clusters as the Wigner Seitz radius r_s (characteristics of the material), denoted as r_0 in the case of nuclei. Each fermion thus occupies the same volume $(4/3)\pi r_s^3$ and the average density of these systems is $\rho \sim 3/(4\pi r_s^3)$ independent of the system size. The parameters r_0, r_s thus play a key role in fixing the characteristic scales in these systems and we can use them for comparison using properly scaled variables, as we shall see below. For example, the typical distance between constituents amounts to about 1.5-2 r_s . The Fermi gas picture also provides a simple energy scale in terms of r_s through the Fermi energy $\epsilon_F = (\hbar^2/2m)k_F^2$ (with $k_F = (3\pi^2\rho)^{1/3} = (9\pi/4)^{1/3}r_s^{-1}$ and $m = m_n, m_e$).

Another interesting, and deeper, similarity concerns the validity of mean field in both systems. The free nucleon-nucleon interaction is known to be strongly repulsive at short range [13], which makes a mean field theory a priori questionable. But the strong Pauli correlations in nuclei significantly suppress low energy scattering. This renormalizes, in a nuclear medium, the interaction to an effective one, following the well known Brueckner picture. The short distance repulsion is then highly suppressed and the effective nucleon-nucleon interaction smooth enough to justify a mean field picture [13]. In nuclear physics the so called Skyrme interactions, which integrate in an effective way, these Pauli correlation effects on a basically zero-range bare interaction, have thus become a standard microscopic tool for decades, because of their simplicity and because of the many successes they have allowed, at least for stability valley nuclei, for a recent review see [7]. As can be seen from table 1 the Skyrme interaction appears as a density functional, mostly local, non-locality being usually assumed in terms of a gradient expansion.

A somewhat similar reasoning applies to metal clusters. The general atomic problem is of course singular (due to the point charge of the atomic nucleus). However, only a limited number of valence electrons actually take part in the binding of molecular systems or clusters. This is especially true in the case of simple metals, in which the valence shell is well separated from core levels and remains usually little bound. Valence electrons can thus easily be delocalized to form the rather "soft" bonds characteristics of metals. It should, by the way, be noted that this also allows a proper (and simple) packaging of the effect of the core electrons into a so called pseudo potential: this reduces the many-electron problem to the treatment of the valence electrons only, in a reasonably smooth ionic background [12]. This again provides a favourable situation for a mean field treatment. The success of the many calculations based on Density Functional Theory (DFT), even in its simplest Local

Density Approximation (LDA) version, constitutes a typical proof of the reliability of the mean field approach.

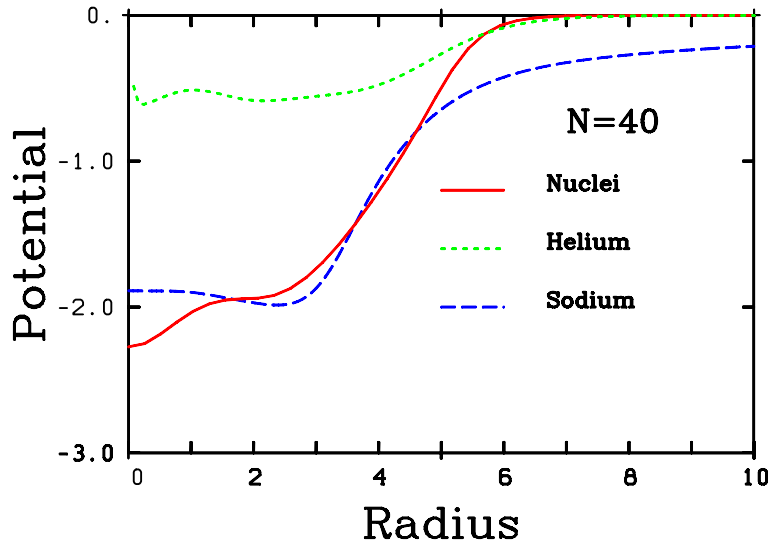


Figure 2. The mean-field potentials for a Na cluster, a nucleus and an helium droplet, with 40 particles (neutrons only in the nuclear case). Natural units are used: lengths in units of r_s and potentials in units of ϵ_F .

In order to quantify this similarity of the mean-field treatments in nuclei and metal clusters we present a comparison of how they look like in systems of comparable "sizes" in Figure 2. We have taken as example the test case of a Na_{40} cluster and of the ^{78}Sr nucleus (with 40 neutrons). The case of an helium droplet with 40 ^3He atoms (representing the third class of Fermi liquid droplets) is also shown for completeness. The comparison is interesting in many respects. The first aspect to be noted is that all three systems fit into one single figure, which means that they have about the same scales when expressed in natural units. They indeed exhibit the same spatial extension, a scale which is directly connected to the "saturation scale" given by $r_{0,s}$. But of course some differences also show up, for example in the depth of the potential wells and in the asymptotic behaviors. The depth of the cluster and nucleus potential wells are in fact comparable while the helium droplet exhibits a much more shallow potential well. This directly reflects the faintness of the interaction between two He atoms. On the other hand, the helium droplet and the nucleus share the same asymptotic behavior, typical of a system dominated by a relatively short-range interaction. The cluster, in turn, exhibits a typical long-range Coulomb behavior. Up to details, the comparison nevertheless shows an overall similarity between the various systems.

Nuclei	$h[\varrho] = -\nabla \frac{\hbar}{m^*(r)} \nabla + t_0 \varrho + t_3 \varrho^{1+\sigma} + t_{12} (\nabla \varrho)^2 + \int \frac{\varrho_p(r')}{ \mathbf{r}-\mathbf{r}' } d\mathbf{r}' + \dots$ $\frac{\hbar^2}{2m^*} = \frac{\hbar^2}{2m} + \alpha \varrho$
Clusters	$h[\varrho] = -\frac{\hbar^2}{2m} \Delta + \int \frac{\varrho(r')}{ \mathbf{r}-\mathbf{r}' } d\mathbf{r}' + U_{xc}[\varrho] + U_{\text{ext}}(\mathbf{r}, t)$

Table 1. One-body Hamiltonian used in mean field calculations in nuclei (Skyrme like interaction), and metal clusters (DFT LDA) In nuclei the density ρ represents the neutron and/or proton density, the latter entering the coulomb interaction alone (ρ_p). In clusters the density is the electronic one. In the case of cluster electrons an important contribution comes from the exchange correlation potential $U_{xc}[\rho]$ which can be treated in the simplest LDA approximation. The external potential $U_{\text{ext}}(\mathbf{r}, t)$ typically refers to the fields as generated by ions or a possible external field (laser, by passing ion...). In the case nuclei one has to introduce an effective mass m^* as indicated, which again depends on the density.

3.2 More on the theory of nuclei and metal clusters

In the immense majority of practical cases the mean-field calculations based on the one-body hamiltonians presented in table 1 are done at quantum level (that was the case of the calculations performed in Figure 2). Each particle (nucleon, electron) is then attributed a one particle wavefunction $\phi_i(\mathbf{r})$, from which one deduces the single particle density matrix $\hat{\rho}(\mathbf{r}, \mathbf{r}')$ and the local one-body density $\varrho(\mathbf{r}) = \hat{\rho}(\mathbf{r}, \mathbf{r}) = \sum_i |\phi_i(\mathbf{r})|^2$ (where the summation runs over all particles). The one-body wavefunctions then follow an effective Schrödinger equation

$$i \hbar \frac{\partial |\varphi_i \rangle}{\partial t} = h[\varrho(\mathbf{r})] |\varphi_i \rangle \quad (1)$$

with an effective single-particle Hamiltonian h expressed as a functional of the density $\rho(\mathbf{r})$, as given in table 1 for nuclei and metal clusters. This mean field equation can be recast in the well known equivalent matrix form

$$i \hbar \dot{\hat{\rho}} = [h, \hat{\rho}] \quad (2)$$

There also exist semi-classical approximations to this quantum scheme, which can be "formally" obtained by transforming the density operator $\hat{\rho}$ into a one-body phase space distribution $f(\mathbf{r}, \mathbf{p}, t)$, which becomes the basic ingredient, and the commutator into Poisson brackets:

$$\begin{aligned} \hat{\rho}(\mathbf{r}, \mathbf{r}') &\longrightarrow f(\mathbf{r}, \mathbf{p}, t) \\ [\cdot, \cdot] &\longrightarrow \{\cdot, \cdot\} \end{aligned} \quad (3)$$

This leads to the well known Vlasov equation

$$\frac{\partial f}{\partial t} = \{h, f\} \quad (4)$$

The one-body Hamiltonian has the same expression in terms of the density $\varrho(\mathbf{r})$ as in the quantal form, but the density is now computed from the phase space density as

$$\varrho(\mathbf{r}, t) = \int d^3p f(\mathbf{r}, \mathbf{p}, t) \quad (5)$$

The major interest of the Vlasov approach is that it can be (relatively easily) extended to account for dynamical correlations. Particle-particle scattering effects can indeed be included as a Markovian collision term for the phase space distribution f . This was worked out in great detail in nuclear physics applications [14] and it was also extended to the cluster case. In both cases (nuclei, metal clusters) one ends up with the so called VUU (Vlasov Uehling Ulhenbeck) equation

$$\frac{\partial f}{\partial t} + \frac{\mathbf{p}}{m} \frac{\partial f}{\partial \mathbf{r}} - \frac{\partial V}{\partial \mathbf{r}} \frac{\partial f}{\partial \mathbf{p}} = I_{UU}(\mathbf{r}, \mathbf{p}, t) \quad (6)$$

with the collision term

$$I_{UU} = \int \frac{d^3p_2 d\Omega}{(2\pi\hbar)^3} \frac{d\sigma}{d\Omega} |v_{12}| \{f_1 f_2 (1 - f_3/2)(1 - f_4/2) - f_3 f_4 (1 - f_1/2)(1 - f_2/2)\} \quad (7)$$

where v_{12} is the relative velocity of the colliding particles 1 and 2. The differential cross section $d\sigma/d\Omega$ (function of the scattering angle Ω) is evaluated in the center of mass frame of the two colliding particles. Indices 3 and 4 label the momenta of the two particles after an elementary collision process and we use the standard abbreviation $f_i = f(\mathbf{r}, \mathbf{p}_i, t)$. The collision is supposed elastic (conservation of energy, of total momentum). Pauli blocking factors $(1 - f_i/2)(1 - f_j/2)$ play an important role here, as they force conservation of Pauli principle in the course of fermion collisions. In the ground state, they correctly block all kinematically possible (and thus classically possible) collisions. At high excitation energy phase space opens up: two-body collisions then start to populate it in the course of thermalization. The VUU scheme was very much used in the case of heavy-ion collisions in the Fermi energy domain. As we shall see below it should also be taken into account in the case of metal clusters, especially in the case of energetic processes.

3.3 Multiscale dynamics

Before analyzing properties of clusters (especially dynamical ones) it is interesting to compare nuclear and cluster time scales. We use reduced units in terms of the Fermi gas characteristics of both systems, following the values introduced above (section 3.1). We thus define a basic time $r_{s,0}/v_F$ and energy ϵ_F scale, as built from the Wigner-Seitz radius r_s for clusters and from the parameter r_0 of nuclear radius systematics ($R \sim r_0 A^{1/3}$, with $r_0 \sim 1.12$ fm). For sake of simplicity, but practically with little loss of generality, we restrict the analysis of the cluster case

to Na, thus taking for the Wigner-Seitz radius $r_s = 4a_0$. This leads to $r_s/v_F = 0.2$ fs and $\epsilon_F = 3.2$ eV. Systematics of electronic time scales for other alkalines perfectly match the values obtained in the case of Na. The ionic motion times scale with the square root of the atom mass. In nuclei the basic time and energy scales read $r_0/v_F = 3.3$ fm/c and $\epsilon_F = 40$ MeV. In figure 3 we have plotted times as a function of temperature. It should be noted that this is rather a simple measure for the average excitation energy. The choice of temperature here is practical and does not necessarily imply a full thermalization. It allows, in turn, to overlook, to a large extent, size dependent effects.

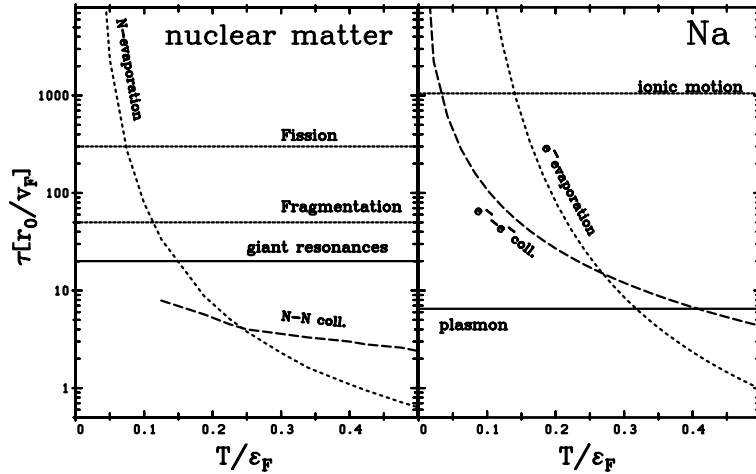


Figure 3. Comparison of relevant times scales in nuclei and sodium clusters. Reduced units are used in both cases to allow a relevant comparison (see text for details). Various times plotted are: plasmon period in clusters (equivalent to giant dipole resonance in nuclei), ionic time scale (comparable to nuclear fission/fragmentation durations), electron (or neutron) evaporation time (equivalent to neutron evaporation time), electron–electron (or nucleon–nucleon) collision time scale.

With this system of reduced units we compare in figure 3 various relevant nuclear and sodium time scales: the cluster plasmon period (equivalent to the giant dipole resonance in nuclei), ionic time scales (comparable to nuclear fission/fragmentation durations), electron (or neutron) evaporation time, electron–electron (or nucleon–nucleon) time scales. The comparison in figure 3 calls for several comments. At first glance one can note a relative similarity between electronic and nuclear time scales. This is especially true concerning the comparable dependences (or independence) of times on temperature. But details differ. One should especially note that the hierarchy of time scales is very different in Na and nuclei. Grossly speaking, nuclear time scales look more similar to each other than cluster ones. There exists a natural hierarchy of well separated time scales in clusters, while nuclear times tend to be much more mixed up. This has important implications in particular from the theoretical point of view. In particular, the lack of a clear time

hierarchy in nuclear dynamics makes a clean adiabatic decoupling of slow degrees of freedom difficult. The simple Born-Oppenheimer treatment of slow degrees of freedom has then to be replaced by the much more involved generator-coordinate-method [15]. In cluster physics the situation is very different due the huge mass difference between electron and ionic masses, which makes electron time scales orders of magnitude smaller than ionic ones. Electrons are thus more responsive than ions: they need to be accounted for in priority in cluster dynamics. It should nevertheless be noted that the separation of electronic and ionic time scales tends to shrink in strongly non-linear situations (in the presence of huge electromagnetic fields).

Differences between nuclear and cluster hierarchies of time scales also concern the times with respect to each other. The case of the role of electron–electron interactions is illustrative here. They become dominant for much higher temperatures in clusters than in nuclei. This means that mean field methods can probably be used at much higher excitation energies in clusters than in nuclei. This is a welcome feature in view of the theoretical difficulties raised by the inclusion of dynamical correlations. Similarly, thermal emission comes into play much earlier in nuclei than in clusters, which again reflects the stronger interference amongst nuclear time scales as compared to cluster ones.

4 A few typical results in statics and dynamics of clusters

After the above brief survey of similarities between nuclei and metal clusters we want now to present a few illustrative examples of properties of metal clusters. The aim here is to describe a few typical observables which have well known counterparts in nuclear physics.

4.1 Shell effects

A basic and well known property of simple metal clusters is the appearance of strong shell effects for example in the abundance spectra [2, 3], similarly to the nuclear case. Shell effects are nevertheless also visible from other observables such as ionization potentials [3]. It is interesting to remind that the identification of strong shell effects in simple (alkaline) metal clusters in the mid 1980's constituted a strong motivation for the study of these systems [16] and the analogy to nuclei was in turn soon recognized and exploited [3]. The analysis of these shell closures was performed at about the same time as their experimental identification [17], primarily within the simple jellium model in which ionic cores are assimilated to an uniform positively charged background. In that simple case electron levels then simply pile up in the mean field generated by their interactions and by the ionic background. After all, the situation, at least for small alkaline clusters, finally strongly resembles to the case of a simple harmonic oscillator. Note that, at variance with the nuclear case there are in simple clusters no sizable spin orbit effects. The series of "magic numbers" (associated to shell closures) is then relatively easy to access.

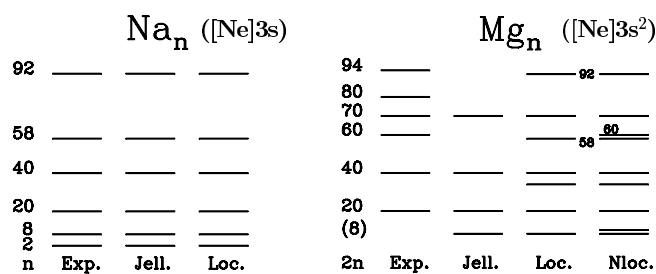


Figure 4. Series of magic numbers for electronic shell closures in sodium (left panel) and magnesium (right panel) clusters. The experimental results are compared to theories of various levels from the simplest jellium one to elaborate ones with an explicit, non local, account (pseudo potentials) of ionic structures (left column of the right panel).

The jellium model was further refined over the years and also replaced by more sophisticated approaches in which one explicitly accounts for ionic structure through the use of pseudo potentials (see section 3.1). This leads, again in the simple case of alkaline metals, to basically similar results, as can be seen in figure 4. The situation nevertheless strongly changes as soon as one considers "less simple" materials. The case of Magnesium clusters was recently studied [18] (remind that magnesium (electronic structure [Ne]3s²) is the nearest "metallic" neighbour to sodium (electronic structure [Ne]3s)). But it turns out that the situation in the case of magnesium is quite different from the one in sodium. Indeed the subshell closure of the 3s orbital in magnesium makes it effectively much less metallic than sodium. This leads to a significantly different sequence of shell closures. In that case of magnesium neither the jellium model nor models explicitly accounting for ionic structure (even sophisticated ones using non local (orbital dependent) pseudo potentials) are able to explain the observed series of magic numbers [19], as can be seen from figure 4.

4.2 Optical response

Let us now consider the case of the optical response as a starter for the analysis of cluster dynamics. Optical (or surface plasmon) response is, as already indicated, a key tool of analysis of metal cluster properties, both in terms of structure and dynamics. The particular softness of the electron clouds in metal clusters make them especially sensitive to a coupling to light. Laser irradiations thus easily lead to a collective oscillation of the electron cloud with respect to the ionic background. The energy scale of the process lies in the visible part of the electromagnetic spectrum: the phenomenon is thus known as the optical response. The optical response is very similar to the giant dipole resonance in nuclei. There are of course differences, es-

pecially what concerns resonance decay mechanisms. For example, in the case of small simple metal cluster the plasmon peak lies in a desert of particle-hole excitations : the mode is thus particularly robust and the signals especially clean. The optical response turns out to constitute an exceptional tool of investigation of cluster structure. We shall illustrate that capability on the example of deformation effects.

Deformation from optical response As the giant dipole resonance in nuclei, the optical response provides a useful tool of analysis of deformation through the splitting of the excitation spectrum. The latter reflects the possibly large quadrupole moment of the cluster. In spherical clusters the optical response is concentrated in one (sharp) peak, which splits into two pieces for axially symmetric deformed clusters. The mode oscillating along the longest axis has the lowest frequency while the mode along the shortest axis has the highest one. Finally, in triaxial clusters one observes three peaks, sorted inversely to the length of the axes.

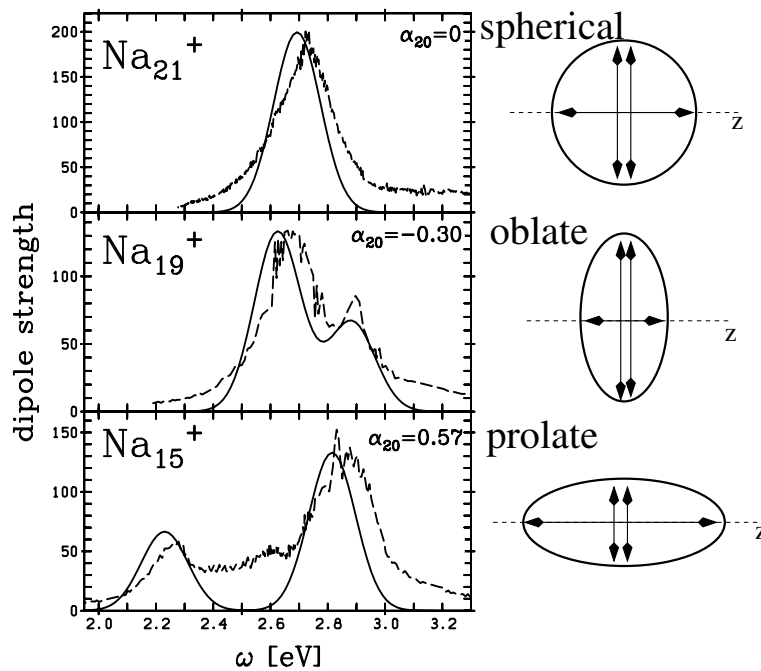


Figure 5. Illustration of deformation splitting of the Mie resonance. Test cases are Na_{21}^+ (spherical), Na_{19}^+ (oblate) and Na_{15}^+ (prolate). The left panels show the optical absorption strengths, experimental from [20] and theoretical results from linearized TDLDA on soft jellium background [21]. The right part sketches the shapes (the deformations are exaggerated to make the point). The lines with arrows indicate the directions of the basic plasmon oscillations. The symmetry axis (z axis) is indicated by a fine dashed line.

This connection is illustrated in figure 5 for three small Na clusters, a spherical one (Na_{21}^+) and two deformed ones (Na_{15}^+ and Na_{19}^+). The case of the prolate Na_{15}^+ cluster (lower part of the figure) is interesting to be discussed in detail. The right part sketches the deformed shape and the corresponding dipole modes. Oscillations along the z -axis (horizontal) are more extended and thus have lower frequency. The orthogonal axes, in turn, are squeezed, yielding higher oscillation frequencies. The left part of the figure shows the optical response (experimental and theoretical), which exhibits a clear splitting into two peaks. The upper peak has twice as much strength as the lower one which reflects the fact that there are two modes orthogonal to the symmetry (z) axis. Theoretical (TDLDA) results agree with experimental data and this can be taken as a clear hint that Na_{15}^+ is a prolate cluster. A similar reasoning holds in the case of oblate Na_{19}^+ . This time the spectrum has a large low energy peak and a smaller high energy peak. And in the case of the spherical Na_{21}^+ the three modes are degenerate and produce one unique, large plasmon peak.

The deformation analysis in terms of plasmon peak splitting works reliably well for small clusters up to $N \approx 40$. In larger clusters strong Landau fragmentation sets on, which blurs the information about deformation splitting [21]. Of course, extreme deformations and/or huge clusters nevertheless still allow one to separate clearly the different branches of the plasmon mode (see for example the experiments on large Au nano-rods [22]). The situation in nuclei is more mixed [23], with, in principle, the same collective splitting of the GDR with deformation. But Landau fragmentation prevails for small nuclei and shrinks only slowly for larger ones. The deformation splitting can thus not uniquely be discriminated for typical ground state deformations and it is only in super-deformed isomers that deformation splitting overrules Landau fragmentation. However, it is extremely difficult to measure the GDR in nuclear isomeric states.

Temperature effects on optical response As previously mentioned, metal clusters are produced at finite temperature in cluster sources. Temperature thus plays a key role in the understanding of cluster properties and optical response does not violate this rule. Systematic experimental studies have actually shown the key importance of temperature effects on the optical response of small metal clusters [24]. Only few theoretical calculations have been performed at finite temperature but they confirm these trends. An example is presented in figure 6, for the optical response of Na_7^+ clusters at various temperatures. The low temperature spectrum exhibits three narrow and well separated peaks. We can identify on this spectrum the collective splitting of the strongly oblate Na_7^+ (see insert in bottom panel). This is complemented in that case by a low energy peak, fragmented by one close $1ph$ state. The effect of temperature is dramatic: the peaks grow broader and the lower double peak merges into one.

Thermal effects at the side of the electrons cannot induce such a broadening simply because the temperature involved here (a few hundreds K at most) correspond to small energies at an electronic scale (remind that $1 \text{ eV} \sim 10\,000 \text{ K}$). It is the thermal ionic motion which is responsible for that behavior. The ionic excitation energies reach down to below 100 K for Na_7^+ [25]. A thermal excitation of several

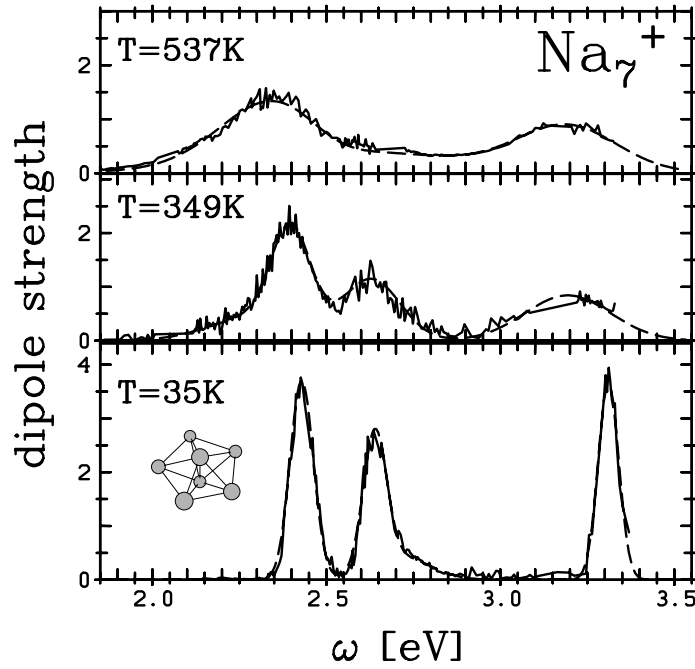


Figure 6. Photo-absorption strength for Na_7^+ at three different temperatures as indicated. The configuration is indicated in the lowest panel. Data taken from [24].

hundreds of K thus excites many ionic eigenmodes to rather large amplitudes. The cluster then undergoes substantial thermal shape fluctuations which take place on a time scale (hundreds of fs) much longer than the one associated to the plasmon response (a few fs). Thus each member of the thermal ensemble with its different deformation will contribute a different spectrum to the total optical response. These spectra finally all add up incoherently to rather broad peaks.

4.3 Photoelectron spectra

The analysis of the kinematic characteristics of electrons emitted after a cluster irradiation also constitutes a key tool of analysis of cluster properties. In the low energy domain, namely for moderate irradiations, it gives access to single electron properties. Indeed photoelectron spectra (PES) display the kinetic energies E_{kin} of the emitted electrons which provides the binding energies E_{bind} of electronic levels through the simple relation $E_{bind} = E_{kin} - \hbar\omega$ (ω being the laser frequency) at least in the case of single photon processes (namely for laser frequencies above cluster ionization potential). The case of multiphoton processes is more involved. It implies

complex dynamical processes in which a simple and direct link to structural aspects (E_{bind} in particular) is blurred.

The low energy domain An example of photoelectron spectra is presented in figure 7 in the case of two medium size sodium clusters (Na_{41}^+ and Na_{93}^+). Comparison between experiment and theory is presented on that occasion. The calculations have been performed at an effective mean field level (TDLDA) comparable to Skyrme Hartree-Fock in nuclear physics. The figure allows to identify several peaks from the spectra, which can be attributed to well defined electronic shells. The calculations lead to a comparable sequence of peaks, although sometimes with different relative weights. The theoretical analysis is furthermore separated in two components, along and perpendicular to the laser polarization axis, which is a rudimentary way to provide an access to the angular distribution of emitted electrons. Not surprisingly one observes that the electron orbitals couple selectively to the laser, as a function of their spatial extension along (or perpendicular to) the laser polarization axis. This by the way provides an a posteriori confirmation of the level assignment of the various observed peaks. More detailed investigations, especially in terms of angular distributions of emitted electrons would here bring further complementing information. We shall discuss that aspect below, in the case of a more violent irradiation process (section 4.4).

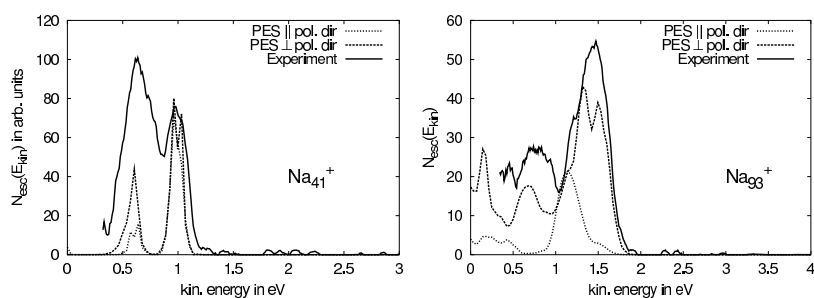


Figure 7. Comparison of experimental photoelectron spectra [26] with theoretical ones in the case of two medium size sodium clusters (Na_{41}^+ and Na_{93}^+). A rudimentary angular analysis is also indicated in the theoretical case by separating electron spectra along and perpendicular to the laser polarization axis.

Photoelectron spectroscopy in the multiphoton regime Let us now consider the case of larger laser intensities. Figure 8 shows the PES of Na_9^+ for two different laser intensities around the transition to the high field regime. As can be seen from the figure, the lower laser intensity still resolves the detailed single-electron states in repeated sequences. The repetition process corresponds to processes involving more and more photons and are thus suppressed accordingly. A moderate enhancement of

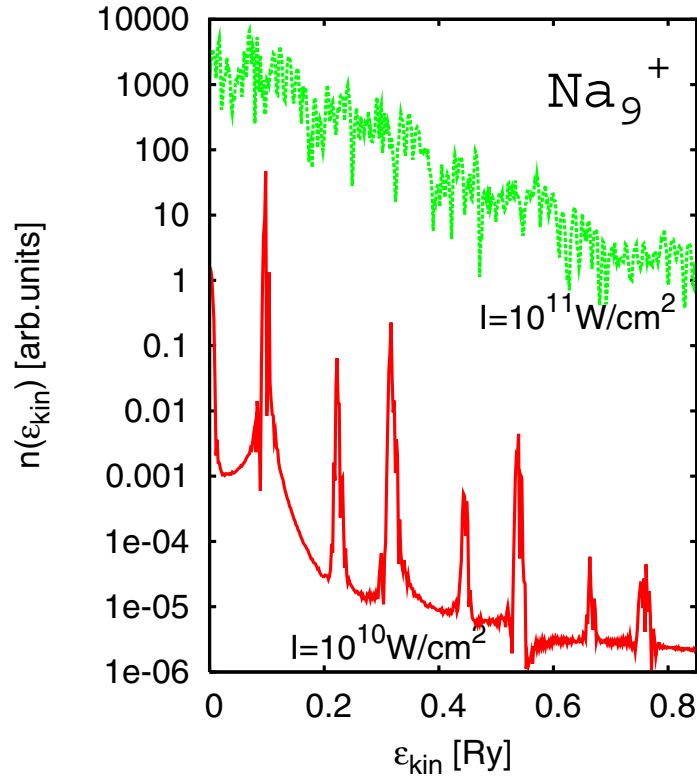


Figure 8. Photoelectron differential cross section (arbitrary units) of Na_9^+ at two intensities as indicated. A short laser pulse with FWHM = 25 fs was used.

the laser intensity by an order of magnitude suffices to wipe out these structures. A more or less smooth curve then emerges which can be nicely fitted to an exponential decrease. The smooth pattern persists, of course, for even larger intensities. It is then interesting to analyze the origin of these smooth pattern, a question which is still debated. One could *a priori* interpret this exponential decrease as a signal of thermalization of the electron cloud. But this argument is not applicable to short laser pulses, as is the case here, because thermalization can hardly play a dominant role when such short time scales are involved. But without arguing in terms of thermalization one can also note that together with the dramatic changes in the pattern of the PES one spots an equally dramatic increase in the ionization. This large increase in net charge at the cluster site has a side-effect on binding. Indeed, the growing Coulomb force (due to charging), leads to extra binding, which globally down-shifts electronic single particle energies by the same amount. This is a dynamical process, which leads all levels to be smeared and eventually generates the smooth pattern seen for the higher intensities. This process does also deliver an exponential decrease of the PES [27]. A better indicator of thermalization would in

fact be provided by the (more detailed) analysis of electron emission in terms of the angular distribution of the emitted electrons. This will be discussed in section 4.4.

The PES change pattern when going to larger systems. Indeed, the larger the system, the denser the density of electronic states, which inhibits a detailed resolution of separate single electron states, and this even at moderate excitations. At best, one can expect step like structures indicating bands of occupied states. Such behaviors were observed in the case of C_{60} for short, moderate pulses [28] and for large Ag clusters on substrate [29]. More recently were also published measurements on Na_{93}^+ from [30], which show smooth trends throughout. These results were interpreted as due to thermal emission. We have thus computed PES for Na_{93}^+ for a variety of laser intensities (but fixed photon frequency and pulse width). At low intensity we observe the expected step like pattern. At larger laser intensity PES exhibit smooth pattern with nearly exponential decrease. The PES can then be simply characterized by the slope of the exponential decrease. The criterion is unambiguous at large intensity but requires some caution at lower intensities because of the step like pattern. But it turns out that the ‘staircases’ have in fact all the same step height (on logarithmic scale). Their envelope is thus a straight line to which it is easy to associate an exponential decrease and one can extend the simple slope characterization to any laser intensity. This allows a direct comparison to experimental data.

The experiments in [30] were done for rather long pulses with a FWHM of about 200 fs. For such long pulses one can expect to see pattern related to electron electron collisions, beyond mean-field. Nonetheless, it is interesting to compare TDLDA (mean-field) results with those measurements in terms of global properties such as net ionization and the slope of the PES, as done in figure 9. Note that for such long pulses one has also to account for ionic motion which sizably alter the sequence of electronic levels and thus the PES. This effect was of course taken into account in the calculations presented in figure 9. The calculations reproduce the net ionization (number of emitted electrons N_{esc} within a factor of two, as well as the growth with laser intensity. This can be considered as a good agreement in view of the fact that ionization also sensitively depends on the pulse shape, an aspect which is always hard to account for precisely when comparing experimental and theoretical results. Calculations use here a cosine² pulse profile while the experimental profile is not so well known, probably having longer tails. The results for the slopes (lower part of figure 9) are also encouraging in size and in trend. Similar trends were reported in [31] in the framework of a Vlasov-LDA approach. The remaining differences between the calculations and the experimental results are thus probably to be attributed to the lack of account of electron electron collisions (overlooking details of laser pulse shape, as mentioned above or even cluster temperature control).

4.4 Angular distributions

Besides the kinetic energy, one can also measure the angular distribution of emitted electrons, a quantity which also carries a lot of interesting information, both for structure and dynamical questions. In the case of laser irradiation one expects

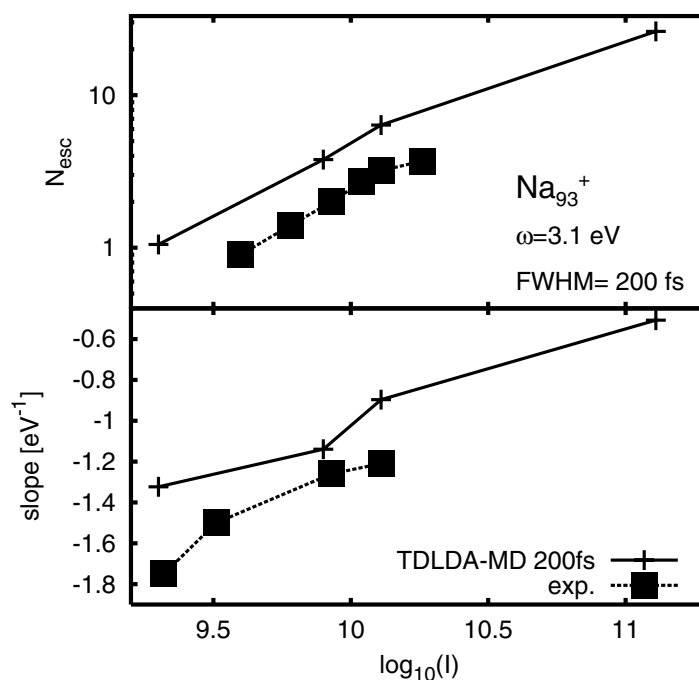


Figure 9. Global properties of emission from Na_{93}^+ , total number of emitted electrons (gain in ionization) in the upper panel and slope of the PES in the lower panel. The laser parameters were $\omega_{\text{photon}} = 3.1$ eV and pulse length FWHM = 200 fs. Results are drawn versus intensity (as $\log_{10}(I)$ with I in units of W/cm^2). Results from TDLDA-MD are compared with the experimental results of [30] using comparable experimental conditions.

electrons to be emitted preferentially, at least to some extent, along laser polarization axis. In fact the amount of anisotropy somewhat depends on the experimental conditions (characteristics of laser pulse in particular). One may even measure simultaneously both angular distributions and kinetic energies of emitted electrons (see left panel of figure 10 for an example).

There are unfortunately only few available experimental data on angular distributions. An example is shown in figure 10. The left panel exhibits a combined kinetic energy and angular distribution measurement. The system under study is a W_4^- cluster anion irradiated by a low-intensity ns laser at a frequency of 4 eV. The anion (negatively charged cluster) has a low ionization threshold around 1.6 eV, much lower than the monomer evaporation threshold (larger than 7 eV). Thermal ionization is thus strongly favored over monomer evaporation in this case. The competition remains, though, between direct (in particular one-photon processes in such an anion) and thermal electron emission. The extremely long laser pulse (as compared to typical electronic or even ionic times) nevertheless gives thermaliza-

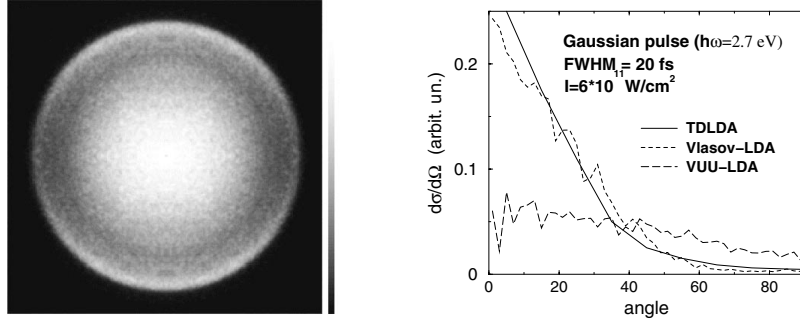


Figure 10. Left panel: 2D equi-density plot of kinetic energy spectra and angular distribution from a W_4^- cluster anion after irradiation with a laser of frequency 4 eV. The emission angle is mapped in terms of polar coordinates while the kinetic energies grow with radial distance from the center of the plot. The gray scale indicates flux: high emission shines white. The laser polarization is along the vertical axis [32]. Right panel: angular distribution of emitted electrons computed in quantum TDLDA (full), semi-classical Vlasov-LDA (short-dashed), and VUU with collision term (long-dashed). Test case is Na_{41}^+ with ionic structure. Laser parameters are indicated in the figures. The angle is defined relative to the laser polarization axis.

tion through electron-electron collisions good chances to be activated and efficient. One thus expects a significant contribution from thermal emission. This is indeed what is observed in figure 10, where light grey indicates large emission and dark grey low emission. The broad central spot can be associated with thermal (isotropic) emission. The kinetic energy spectra (not directly visible in the figure) indeed confirm the correct trend $\propto \sqrt{\varepsilon_{\text{kin}}} \exp(-\varepsilon_{\text{kin}}/T)$ [32]. But at larger kinetic energies (which correspond in this representation to larger radial distances) one can also spot a non-isotropic component in the emission. It is directed along the laser polarization axis and this is thus clearly a signal from a direct emission process competing with thermal (isotropic) emission.

A full description of such processes should thus account for electron-electron collisions in order to properly access the isotropic component of the electronic emission. Such an extension of the theory would thus allow to cover both regimes, namely direct emission as well as thermal evaporation. A way to include such effects in the TDLDA approach is to rely on the semi classical version of the theory, properly extended by a collision term to account for electron electron collisions [33, 34], in the spirit of similar extensions worked out several years ago in nuclear physics [14] (see the discussion in section 3.2). The semi-classical approach

of course requires sufficiently high excitation, but, as in the nuclear context, that is the typical situation for thermalization to play a role at all. The right panel of figure 10 shows an example of angular distributions as obtained from such a VUU calculation. It is compared to pure mean-field results (a quantum TDLDA one and a semi classical Vlasov-LDA one). Note that at variance with the left panel of figure 10 the distribution has been integrated over final kinetic energy (making it a differential cross section, not a doubly differential one). It is noteworthy first that TDLDA and Vlasov nicely agree in that excitation regime. Both show an emission clearly peaked along the laser polarization, a behavior which is typical of direct emission. But the electron-electron collisions in VUU also lead to a sizeable isotropic component in the angular distribution. Not surprisingly, the delayed emission of the thermalized electrons has lost memory of the original polarization axis. One thus obtains a much smoother angular distribution, as can be seen on the VUU curve of the right panel of figure 10. The distribution is nevertheless not perfectly isotropic. There remains a sizeable fraction of directly emitted electrons for the chosen conditions. The branching between direct and thermal emission in fact sensitively depends on the details of the excitation. Systematic studies of these influences could thus deliver valuable information on the underlying dynamics. But these studies have yet to be worked out, both theoretically and experimentally.

5 Conclusions

Metal clusters and atomic nuclei are often compared. They indeed share several common trends. They both constitute finite droplets of fermi liquids which is one of the sources of the similarities. Both can furthermore be well described by effective mean field approaches. The DFT/LDA in the case of clusters is a typical such approach, and it should be compared to Skyrme Hartree-Fock theory of nuclei. We have presented in this contribution a few structure and dynamical properties of metal clusters, focusing on properties of metal clusters which have similar counterparts in nuclei. We have given a brief presentation of basic experimental observables, as typically attained in cluster experiments. We have discussed the occurrence of magic numbers in cluster abundance spectra, in a way very similar to the nuclear case. We have then discussed a few properties of the optical response, the cluster analogon of the nuclear giant dipole resonance. We have shown that the optical response provides a useful tool of investigation of cluster properties. This holds especially true for the analysis of cluster shapes, even if thermal effects may blur the picture in some cases. We have finally turned ourselves towards the analysis of photoelectron spectra both in the linear and non linear domains. We have shown that moderate irradiations give access to single electron energies, while more violent irradiations lead to a variety of dynamical scenarios raising debated questions such as the occurrence (or not) of thermalization at the side of electrons

Acknowledgements

The authors thank the french-german exchange programs PROCOPE, Institut Universitaire de France, Humboldt fundation and French ministry of research (Gay-Lussac award) for financial support during the realization of this work.

References

1. , D. Pines and P. Nozières, *The Theory of Quantum Liquids*, (W A Benjamin, New York, 1966)
2. M. Brack , *Rev. Mod. Phys.* **65** (1993) 677.
3. W. A. de Heer , *Rev. Mod. Phys.* **65** (1993) 611.
4. G. F. Bertsch and R. A. Broglia, *Oscillations in Finite Quantum Systems*, (Cambridge University Press, Cambridge, 1994).
5. U. Näher et al, *Phys. Rep.* **285** (1997) 245.
6. R. M. Dreizler and E. K. U. Gross, *Density Functional Theory: An Approach to the Quantum Many-Body Problem*, (Springer-Verlag, Berlin, 1990).
7. M. Bender and P.-H. Heenen and P.-G. Reinhard, *Rev. Mod. Phys.* **75** (2003) 121.
8. P.-G. Reinhard, Y. Gambhir, *Ann.Phys. (Leipzig)* **1** (1992) 598.
9. P.-G. Reinhard, *Ann.Phys. (Leipzig)* **1** (1992) 632.
10. P.-G. Reinhard, O. Genzken, M. Brack, *Ann. Phys. (Leipzig)* **5** (1996) 576.
11. S. Weisgerber, P.-G. Reinhard, *Ann.Phys. (Leipzig)* **2** (1993) 666.
12. P.-G Reinhard and E Suraud, *Introduction to Cluster Dynamics*, (Wiley, New York, 2003).
13. P. Ring and P. Schuck, *The Nuclear Many-Body Problem*, (Springer Verlag, New York, Heidelberg, Berlin", 1980).
14. G. F. Bertsch and S. Das Gupta, *Phys. Rep.* **160** (1988) 190.
15. P.-G. Reinhard and K. Goeke, *Rep. Prog. Phys.* **50** (1987) 1.
16. W. D. Knight et al *Phys. Rev. Lett.* **52**(1984) 2141.
17. W Ekaradt , *Phys. Rev. Lett.* **52** (1984) 1925.
18. T. Diederich et al *Phys. Rev. Lett.* **86** (2001) 4807.
19. Ll. Serra, P.-G. Reinhard and E. Suraud, *Euro. Phys. Journ. D* **18** (2002) 327.
20. H. Haberland and M. Schmidt, *Euro. Phys. J. D* **6** (1999) 109.
21. V. O. Nesterenko, W. Kleinig and P-G Reinhard, *Euro. Phys. J. D* **19** (2002) 57.
22. C. Sönnichsen, T. Franzl, T. Wilk, G. von Plessen and J Feldmann, *Phys. Rev. Lett.* **88** (2002) 077402.
23. J.A. Maruhn et al, *Phys. Rev. C* **71** (2005) 064328.
24. C. Ellert et al, *Phys. Rev. Lett.* **75** (1995) 1731.
25. P.-G. Reinhard and E. Suraud, *Euro. Phys. Journ. D* **21**, (2002) 315.
26. G. Wrigge, M. A. Hoffmann and B. von Issendorff, *Phys. Rev. A*, **65** (2002) 063201.
27. A. Pohl, P.-G. Reinhard and E. Suraud, *J. Phys. B*, **37** (2004) 3301.
28. E. E. B. Campbell et al, *Phys. Rev. Lett.* **84** (2000) 2128.
29. J. Lehmann et al, *Phys. Rev. Lett.* **85** (2000) 2921.
30. R. Schlipper, R. Kusche, B. von Issendorff and H. Haberland, *Appl. Phys. A* **72** (2001) 255.
31. T. Fennel, G. F. Bertsch and K-H Meiwes-Broer, *Euro. Phys. Journ. D* **29**, (2004) 367.
32. B. Bagueard, J. C. Pinar, C. Bordas and M. Broyer, *Phys. Rev. A* **63** (2001) 023204.
33. A. Domsps, P.-G Reinhard and E. Suraud, *Phys. Rev. Lett.* **80** (1998) 5520.
34. E. Giglio, P.-G Reinhard and E. Suraud, *J. Phys. B* **34** (2001) 1253.